Optimizing Electric Motor Controls with Dynamic Motor Drive

Dr Zhiqian **Chen**; Paul **Carvell**; Dr Adya **Tripathi**; Dr Matthew **Younkins**; Dr Zakirul **Islam**; Dr Siyu **Leng**; Amnish **Singh**; Anastasios **Arvanitis**; Andrew **Phillips**
Tula Technology, San Jose, California, USA

Contact: chenz@tulatech.com

Content

Abstract

Improving the efficiency of battery-electric vehicle powertrains is a key to transportation electrification. Although the peak efficiencies of electric motors exceed 90%, practical drive cycles and powertrain architectures frequently operate outside of the peak efficiency region. Furthermore, the most efficient motors use extensive amounts of rare earth magnets, which are expensive and have limited sources of supply.

Tula's Dynamic Motor Drive (DMD®) control strategy mitigates the light-load efficiency losses of electric motors while simultaneously reducing or eliminating the reliance on rare-earth materials. By using the DMD pulse density strategy for electric motor control, inverter losses and core losses are reduced. This paper details the optimization of

motor design for this new control paradigm, the control methodology used to achieve those gains, and the experimental results of that system in use.

1 Motor Efficiency is Vital for Automotive Electrification

Automobiles are a major pollution contributor, producing significant amounts of nitrogen oxides, carbon monoxide, and other pollutant emissions. The World Health Organization (WHO) estimated that in 2012 air pollution was responsible for 7 million premature deaths, including 600,000 in Europe alone [1]. Toxicity is not limited to chemicals; the WHO also concluded that vehicular noise caused in large part by combustion engines was responsible for over one million of life lost annually in western Europe [2].

Transportation byproducts are also driving climate change at a massive scale. Increasing temperatures and anomalous trends in weather events are becoming common and are in large part caused by greenhouse gas emissions. A report from NASA claims that recent increase in atmospheric CO_2 has already reached 50% over pre-industrial level and without concerted efforts will increase much further [3].

Electrification of the automotive fleet can be part of the solution to these environmental problems. Even with electric vehicles, though, making them as efficient as possible is still paramount, as the electrical grid will be largely powered by fossil fuels for the foreseeable future. Although collaborative actions to reduce fossil fuels in the electrical grid have gained traction, nevertheless, in 2019, over 17 gigawatts of new coal power plants were approved to begin being built [4]. With the incresing popularity of battery-electric vehicles (BEVs), this number may even increase in the future. To prevent this from happening, every reasonable action must be taken to mitigate the impact of BEVs on our world. We must improve the efficiency of BEV powertrains. Although the peak efficiencies of electric motors exceed 90%, practical drive cycles and powertrain architectures frequently operate outside of the peak efficiency region. Further improvement throughout the operating regime is required.

Unfortunately, one of the key methods that has been used in recent years to improve the efficiency of electric powertrains is to increase the content of rare earth metals. Although this strategy is effective in producing efficiency gains for some of the roughly 7 million electric vehicles in use today, it is not likely to be an adequate and economical solution in the future when the entire 1.4-billion-unit automotive consists of electric vehicles. It is not clear that mining and recycling can supply with a reasonable price the rare earth metals required for an electric vehicle fleet two hundred times larger than the current fleet of BEVs.

Sources of economically recoverable rare earth metals are concentrated in only a few locations worldwide. Among them Neodymium and Dysprosium are considered to be of critical importance and risk [5]. It is estimated that the demand in the next decade for these metals will increase by a factor of 248% and 215%, respectively [6][7].

Although rare earth metals will be a key enabler of our vehicle conversion, we cannot rely exclusively on rare earth metals being affordable in the future.

2 Tula's Dynamic Motor Drive

Tula Technology, founded in San Jose, California in 2008, has a history of improving the efficiency of the automotive fleet with Dynamic Skip Fire (DSF®) technology. This technology implements new control strategies on conventional engines to improve efficiency and has been implemented on General Motors' products since 2018. The company has successfully navigated from startup and is now a profitable entity in series production.

Tula recognizes that it is critical to reduce the negative impact the automotive fleet has on the world, even for powertrains that are based on batteries and electric motors. To that end, Tula has been working to optimize the system efficiency of BEVs algorithmically and has successfully developed the concept of Dynamic Motor Drive (DMD®) [8].

2.1 Dynamic Motor Drive Strategy

A typical motor efficiency map for traction drive is shown in Fig. 1. Depending on the motor speed and the output torque, the motor efficiency varies at different operating points. The peak efficiency of 96% is limited to a very small range of speeds and loads. The white line in the graph depicts optimal efficiency points at various speeds.

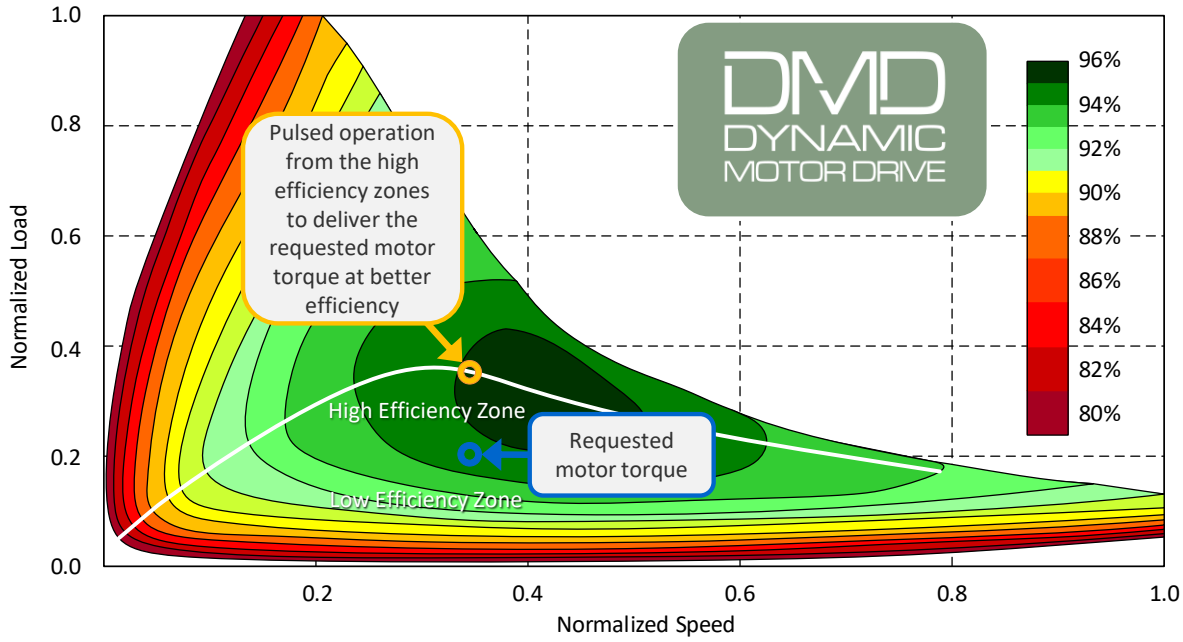

Fig. 1 Concept of Dynamic Motor Drive.

For DMD, the algorithm compares the requested torque with the optimal efficiency line. If it is below the line, the electric motor is operated intermittently at the highest possible electromagnetic efficiency with torque pulses. In the example shown, the optimal efficiency is at 34% of the peak torque, and the requested torque is at 19% of the peak

torque. The controller therefore operates at the optimal efficiency point roughly 19/34 = 56% of the time.

2.2 Power Loss Analysis

DMD strategy is applicable for a variety of types of motors [8]. This work focuses on an increasingly relevant type of motor: a Synchronous Reluctance Motor (SynRM). The production of torque for SynRM's is described by the equation:

$$\tau = \frac{3}{2}P\left(L_d - L_q\right)i_d\, i_q = \frac{3}{4}P\left(L_d - L_q\right)I^2 sin2\delta = kI^2 \qquad \text{Eq. 1}$$

Here, τ, i, L, P, I, δ denote torque, phase current, inductance, number of pole-pairs, current amplitude, and current angle, respectively. Subscripts stand for d-axis and q-axis.

Here, we assume there is no magnetic saturation, i.e., $L_d - L_q$ is constant. This is a reasonable assumption as DMD's algorithms are active at lower loads with less saturation.

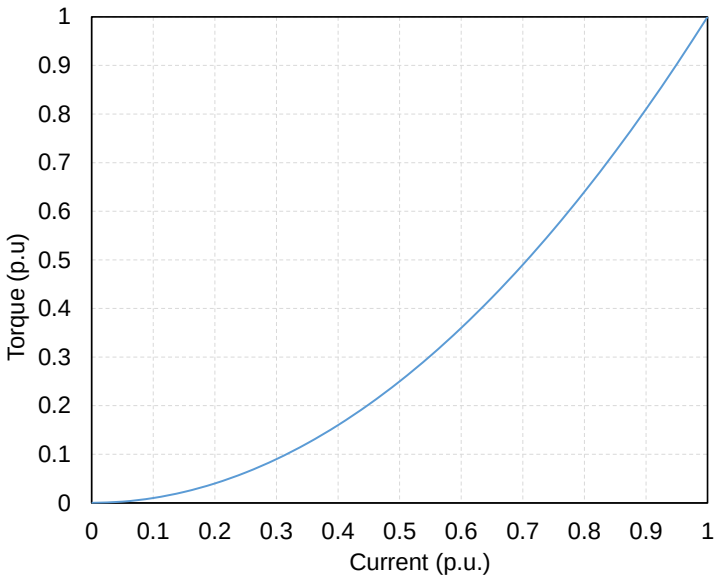

Fig. 2 The ideal relationship between torque and current for SynRM's.

From Eq. 1, it is known that torque is a quadratic function of current amplitude. This relationship is shown in Fig. 2. This type of motor needs relatively more current for low torques, but it does not increase proportionally at high torques. For example, to double the output torque, the current only increases by around 41%.

Advantages of DMD can be maximized when the motor is out of flux-weakening region, where the inverter can be switched off in the periods of low torque during DMD modulation. When the inverter is off, most of inverter and motor losses become zero. However, for the rest of the time, higher torque is output so that the average torque in one modulation period matches the demand. For a motor that has a linear relationship between the power losses and the torque, the final loss is equivalent. For the same

reason, if the relationship is sublinear, then losses will be reduced. Conversely, if the relationship is superlinear, losses will be increased.

For SynRM's, since torque is a quadratic function of current amplitude, the threshold of improved DMD efficiency is also a quadratic function of loss and current. Therefore, it is necessary to clarify the relationship between current and each type of loss.

Inverter conduction loss

For a two-level voltage source inverter, there are usually two types of power losses: conduction losses and switching losses. Conduction loss of transistors can be calculated by Eq. 2 [9]. Conduction loss of free-wheeling diodes can be calculated in a similar manner, which is not discussed here.

$$P_{CON} = V_{CE0}\left(\frac{1}{2\pi} + \frac{1}{8}mcos\varphi\right)I + R_{CE}\left(\frac{1}{8} + \frac{1}{3\pi}mcos\varphi\right)I^2 = aI + bI^2 \qquad \text{Eq. 2}$$

Here, V_{CE0} is the equivalent voltage drop at zero current for bipolar devices, such as IGBT's; $R_{CE}$is the equivalent resistance between collector and emitter for IGBT's, or between source and drain for MOSFET's. m and φ are modulation index and power factor angle, respectively.

Substituting Eq. 1 in to Eq. 2,

$$P_{CON} = \frac{a}{\sqrt{k}}\sqrt{T} + \frac{b}{k}T \qquad \text{Eq. 3}$$

This shows a sublinear relationship for the first term, and a linear relationship for the second term.

In torque modulation of DMD, the motor outputs a high torque with high efficiency, followed by nominally zero torque production that has no electromagnetic losses. In this case, the first term of Eq. 3 decreases from a constant torque output, while the second term does not change. Thus, the overall conduction loss is reduced.

Inverter switching loss

Switching losses can be calculated according to the equation [9]:

$$P_{SW} = \frac{f_{SW}V_{DC}}{\pi V_{ref}I_{ref}}\left(E_{ON}^{ref} + E_{OFF}^{ref} + E_{RR}^{ref}\right)I \qquad \text{Eq. 4}$$

Here, f_{SW}, V_{DC} are switching frequency and DC-link voltage. V_{ref}, $I_{ref}$are reference voltage and current. E_{ON}^{ref}, E_{OFF}^{ref}, $E_{RR}^{ref}$are turn-on, turn-off, and reverse recovery losses, respectively, at reference voltage and current. Since this is a linear function of current, these losses are reduced with DMD.

Motor copper loss

According to Ohm's law, the copper loss in the stator winding is expressed as:

$$P_{Cu} = RI^2 \qquad \text{Eq. 5}$$

Because this is quadratic to current, this type of loss does not change with DMD for SynRM's.

Motor core loss

The two major types of core losses are eddy current losses and hysteresis losses. The eddy current losses are generally calculated with the empirical formula

$$P_w = k_w \delta f^2 B^2 V \qquad \text{Eq. 6}$$

where, considering only fundamental current component, k_w, δ, f, B, V are eddy current coefficient, thickness of lamination, current frequency, maximum flux density, and volume of magnetic material, respectively.

Hysteresis losses can be calculated by

$$P_h = k_h f B^{1.6} V \qquad \text{Eq. 7}$$

where, k_h is hysteresis coefficient [10].

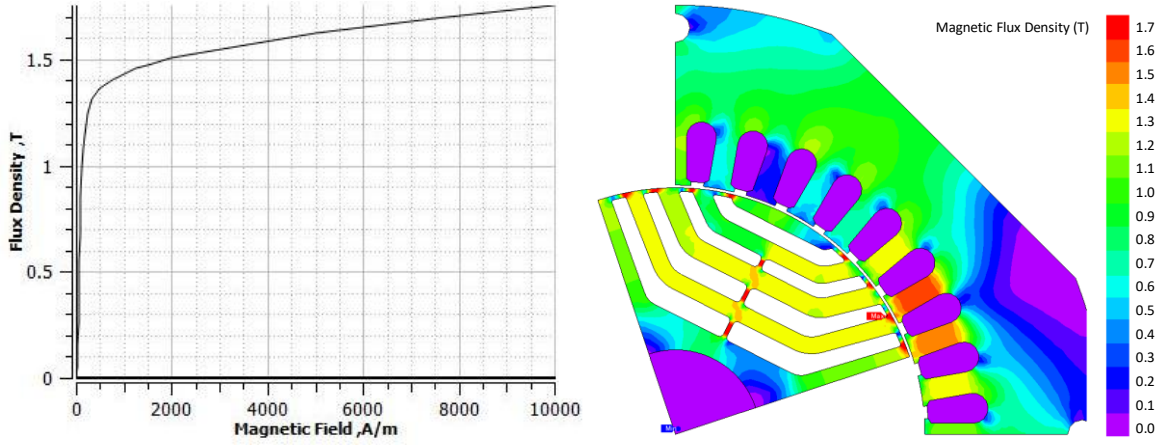

Fig. 3 (a) A typical BH curve of silicon steel; (b) An exemplar motor flux distribution.

A typical B-H curve demonstrating the relationship between current amplitude I and flux density B is shown in Fig. 3(a). It should be noted that the flux distribution is not even in a motor, like the example shown in Fig. 3(b). Some areas are in the linear range, and in these areas the hysteresis losses are reduced in DMD operation. Conversely, other areas have flux densities in the non-lineal range, which shows a sub-linear relationship between flux density and current; and in these areas DMD will reduce both types of core losses. In either case, core losses will be reduced for SynRM's.

Other losses

Friction and windage losses are not affected by torque control methods.

As all losses either remain constant or decrease in the pulsating regime of Dynamic Motor Drive, DMD will improve the efficiency of SynRM's.

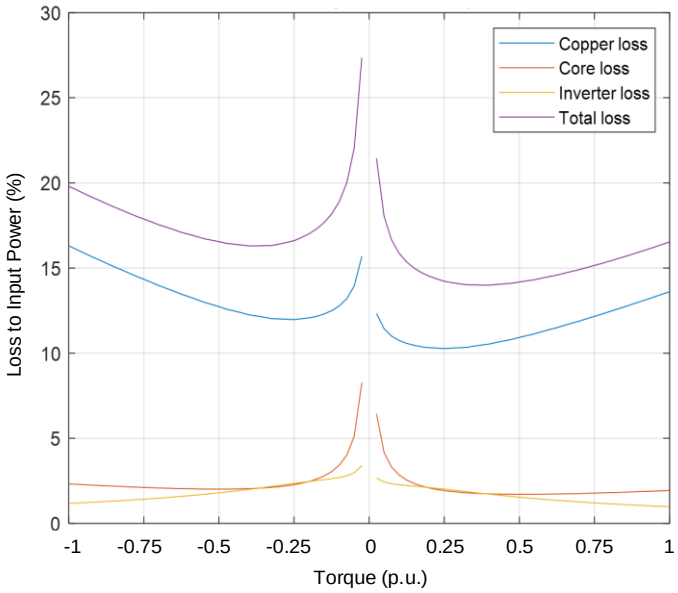

Fig. 4 Breakdown of losses at a speed.

A breakdown of losses into component losses are shown in Fig. 4. The percentage of input power that is lost to inefficiencies varies with torque. The total loss ratio is a convex function with stationary points near +33% of full-scale torque while motoring and -38% of full-scale torque while regenerating, which are the minimum loss points. Operating at these points intermittently helps to improve the motor's efficiency.

Similar analysis indicates Induction Motors (IM) and Switched Reluctance Motors (SRM) also have efficiency gains with DMD. No gains are anticipated for Surface Permanent Magnet Motors (SPM). Interior Permanent Magnet Motors (IPM), which can be considered a hybrid of SPM and SynRM, can exploit the advantages made possible with DMD, particularly if the motor has been designed to use a large proportion of reluctance torque.

3 Synchronous Reluctance Motor Design

To verify the proposed DMD strategy, a 15kW SynRM was prototyped by retrofitting an off-the-self three-phase induction motor with a newly designed rotor. The specifications are shown in Tab. 1.

A multi-objective genetic algorithm (GA) was used to search the rotor parameters, in a multi-physics optimization environment created to deal with the electromagnetic performance as well as the mechanical stress for the maximum speed. The whole

optimization process of this study was comprised of four major steps. The first step was to develop a parameterized model in a finite element analysis (FEA) tool JMAG-designer. The second step was to define the optimization conditions by assigning min-max values of design variables, setting the objectives for minimization or maximization, and defining the limit of selected output parameters. The third step was to run the optimization calculation and select a few top-performing designs from all the candidate designs. The fourth step was to implement the manufacturing tolerances on the top-performing designs to choose the most robust and optimal model.

Tab. 1 Specifications of the designed SynRM.

Parameters	Value
Number of slots	36
Number of poles	4
Stator outer diameter (mm)	208
Rotor outer diameter (mm)	119.4
Stack length (mm)	126.25
Airgap length (mm)	0.55
Rated current (Arms)	16.25
Line-to-line peak voltage (V)	325
Steel grade of rotor	M19 29 gauge

The optimization objectives were set to maximize the torque per ampere current, to minimize the torque ripple, and to minimize the percentage of total harmonic distortion (THD) of the induced voltage. The mechanical stress analysis was carried out for the maximum speed to ensure that the Von Mises Stress do not cross the yield stress of the core laminations. Limits were also set to keep the 5th and 7th line-to-line voltage harmonics below a certain ratio to the fundamental voltage.

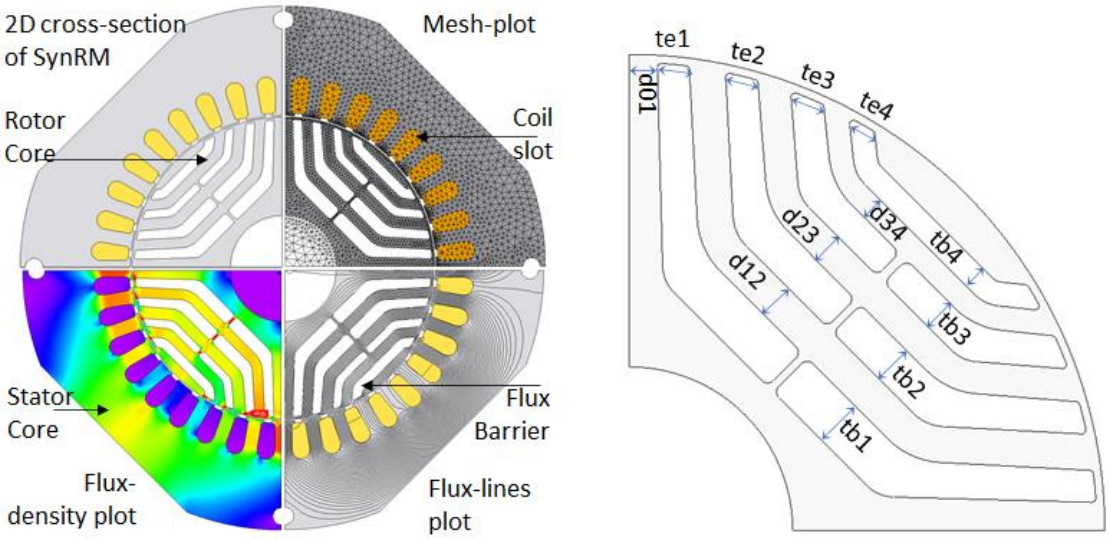

Fig. 5 (a) Cross-section, mesh-plot, flux-line plot, and flux-density plot of a typical SynRM; (b) rotor design parameters of the SynRM model.

Fig. 5(a) shows different types of plots of a typical SynRM. Fig. 5(b) shows the rotor parameters of the SynRM rotor model used as design variables during optimization. It has four flux-barriers. The design parameters were varied within the assigned ranges and used to create candidate designs following the GA.

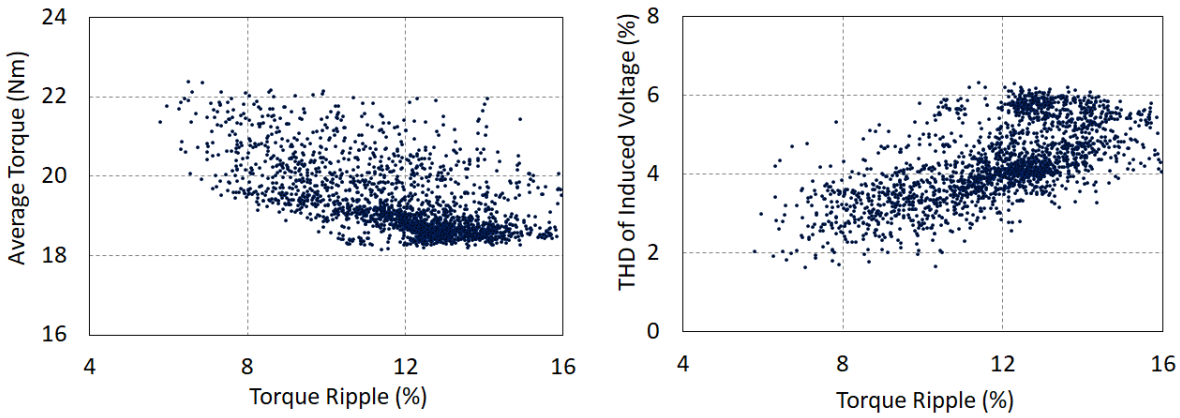

Fig. 6 Scatter plots of the candidate designs: (a) average torque vs percentage of torque ripple; (b) percentage of THD of the line voltage vs percentage of torque ripple.

Fig. 6 shows the scatter plot of the candidate designs. Among them, the optimal designs were selected based on the average torque, torque ripple, voltage-harmonics, etc. Fig. 6(a) shows the average torque vs percentage of torque ripple. Fig. 6(b) shows percentage of THD of the line voltage vs percentage of torque ripple.

Finally, one best model with less sensitivity to tolerance-related parameter variations was selected for prototyping. Its efficiency map is shown in Fig. 7. A picture of the prototyped rotor is in Fig. 8.

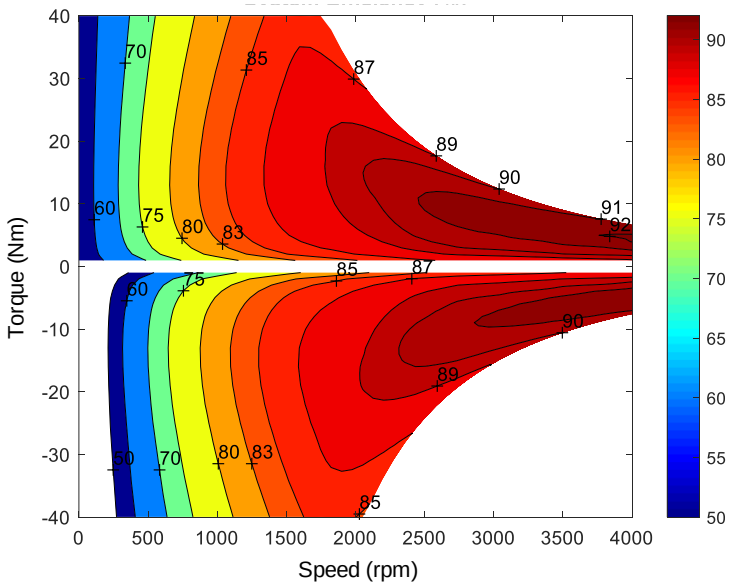

Fig. 7 System efficiency of the designed 15kW SynRM.

Fig. 8 Prototype assembled SynRM.

4 Torque Control Law as Applied to DMD

Torque control law decides how much current is necessary to output the demanded torque, and the ratio between d-axis and q-axis, commonly referred to as the current angle. There are several strategies commonly used:

- Maximum Torque Per Ampere (MTPA) control, sometimes also known as minimum copper loss control. The strategy finds the operating conditions that output the maximum torque under constant amplitude of stator current.
- Maximum Torque Per Loss (MTPL) control optimizes current to reduce all losses. Calibration of this strategy, including creating appropriate control look-up-tables (LUT's), is more difficult as they require loss measurement. Many motors do not exhibit significant differences when comparing MTPA and MTPL.
- Maximum Torque Per Volt (MTPV) control is used in flux-weakening control when both the current constraint and the voltage constraint apply.

For simplicity, MTPA is taken here as an example. It is the predominant strategy used in the low-to-medium speed region. From the mechanical formula of SynRM in Eq. 1, torque is maximized when the current angle is 45^{o}. However, because of magnetic saturation, the relatonship between the maximum torque and current angle becomes a complicated non-linear function, which has no analytical solution.

There are basically two approaches to obtain the MTPA LUT: FEA-based method and experiment-based method. Both are carried out on the 15kW prototype SynRM with the results shown in Fig. 9.

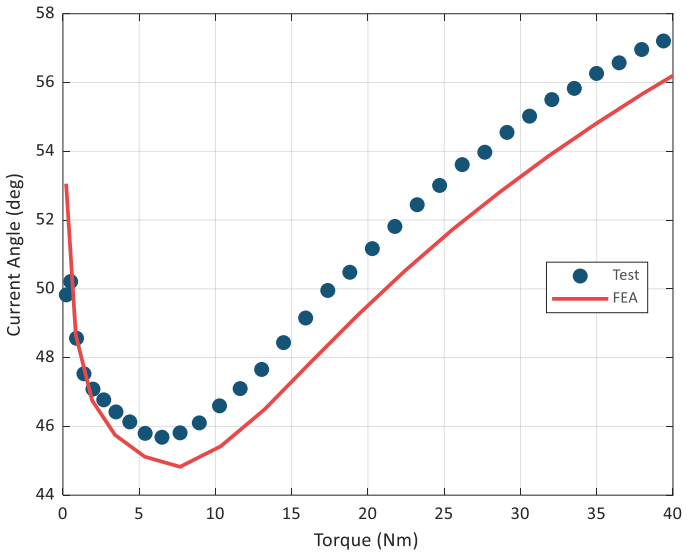

Fig. 9 Current angle of MTPA strategy of the test SynRM.

The results shown in Fig. 9 indicate that FEA results deviate about 1° from test results, as the core loss current is not included in the MTPA analysis. In contrast, the core loss current is always implicitly included in experimental results measuring the total phase current. As such it becomes necessary to use analytical methods to compensate the FEA methods.

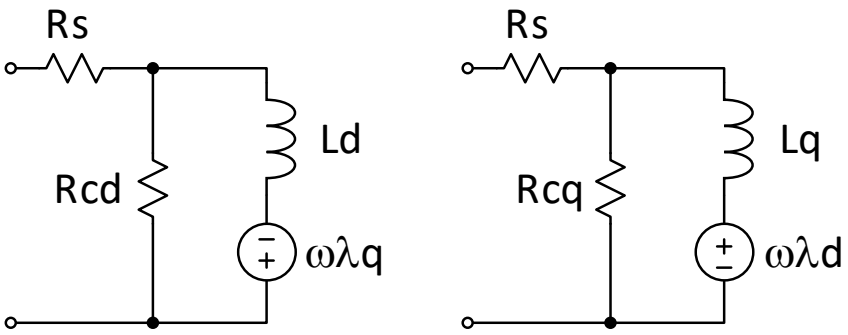

Fig. 10 Equivalent electric circuits of d-axis (left) and q-axis (right) windings.

Fig. 10 shows the electrical circuits of motor's stator windings on d-axis and q-axis, respectively. R_s is the winding resistance. R_{cd} and R_{cq} are the core loss resistances. λ_d and λ_q are the fluxes. For motors with saliency, like SynRM's, the core loss resistance on d-axis and q-axis are not the same. FEA MTPA analysis only uses the currents flowing through L_d and L_q, while experiment measures the currents flowing through R_s.

To correct the results obtained from the FEA model, it is necessary obtain the core loss resistances R_{cd} and R_{cq}. They can be calculated from core loss power P_{cd} and P_{cq} as following:

$$R_{cd} = \frac{\left(\omega\lambda_q\right)^2}{P_{cd}} \quad \text{Eq. 8}$$

$$R_{cq} = \frac{(\omega\lambda_d)^2}{P_{cq}} \quad \text{Eq. 9}$$

It is possible to obtain core loss power from FEA simulation. However, the result is a scalar without distiguishing components on the d-axis and the q-axis. To distribute the scalar core loss into two orthogonal directions, it is scaled according to the flux density in direct and quadrant directions, respetively.

$$P_{cd} = P_c cos^2\,\gamma \quad \text{Eq. 10}$$

$$P_{cq} = P_c sin^2\gamma \quad \text{Eq. 11}$$

Here, γ is the flux angle, i.e.

$$tan\gamma = \frac{\lambda_q}{\lambda_d} \quad \text{Eq. 12}$$

Thus, the core loss currents are estimated using the following equations:

$$I_{cd} = \frac{|\omega\lambda_q|}{R_{cd}} \quad \text{Eq. 13}$$

$$I_{cq} = \frac{|\omega\lambda_d|}{R_{cq}} \quad \text{Eq. 14}$$

Taking core loss current into account, the compensated MTPA curve based on FEA results is shown in Fig. 11, and much better agreement with the experiements can be observed.

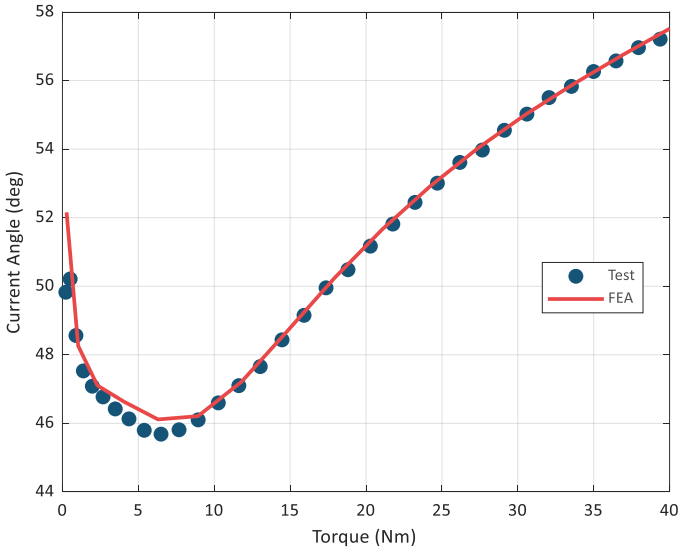

Fig. 11 Current angle of MTPA strategy of the test SynRM.

5 DMD Current Control

Most torque controllers for electric motors are designed to deliver the highest efficiency in steady state conditions. Commonly used strategies include MTPA, MPTL, and MTPV. However, the motors' behavior during transients are rarely studied and optimized, as conventional motor controls do not generally operate heavily at transitions for appreciable portions of the drive cycle. As DMD repeatedly cycles torque on and off to save energy during steady state, efficiency during transients become critical for cumulative efficiency. This section takes an in-depth discussion on the transient performance.

5.1 Torque Rate Limiting at Voltage Saturation

The electric equations of a SynRM on the d-q rotational coordinate are shown in Eqs. 15 and 16. For simplicity, core loss resistances are neglected. The first terms of both equations are the voltage drop on the stator windings. The second terms are the armature reaction. These two types of terms are the voltages necessary to maintain steady state. The third terms are derivative terms, imposed on the windings to increase or decrease the current during transients.

$$v_d = R_s i_d - \omega L_q i_q + L_d \frac{d}{dt} i_d \qquad \text{Eq. 15}$$

$$v_q = R_s i_q + \omega L_d i_d + L_q \frac{d}{dt} i_q \qquad \text{Eq. 16}$$

To better understand the functions of these three types of terms, they are depicted into a vector diagram as Fig. 12. The three vectors $R_s \boldsymbol{i}$ (dashed green), $\omega L \boldsymbol{i}$ (dashed orange), and $L d\boldsymbol{i}/dt$ (dashed blue) corresponding to the three types of terms are added to decide the final voltage output $\boldsymbol{v}$ (dashed red).

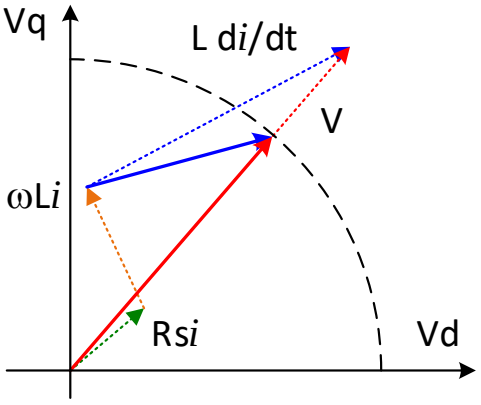

Fig. 12 Vector diagram of voltages.

To turn the motor torque on and off in DMD, a very fast response speed is desired to realize high modulation frequencies. Such a steep change of current requires high

derivative terms of voltage. This usually makes the total voltage exceed the DC-link voltage available, which is depicted in the graph as the black dashed-line circle. To deal with cases of saturation, a common practice is to reduce the amplitude of the vector to contain it within the DC voltage, but keep the vector angle the same (solid red). It should be noted that the voltage-drop due to resistance (green) and armature reaction (orange) terms remain when the voltage saturates. Therefore, reducing the voltage amplitude without changing the angle results in changing both the amplitude and angle of the derivative term as shown in the figure as solid blue.

When modulating the torque, it is also optimal to maintain the ratio between d-axis and q-axis current, and thus tracking the MTPA curve, so that the motor is always working at the optimal efficiency. A well-designed current controller adjusts the voltage output so that the actual current follows the commanded current with minimal error. Any strategy with wide enough bandwidth, whether a proportional-integral (PI) controller, a deadbeat controller, or a sliding-mode controller, can accomplish the task without any issue, provided the voltage does not saturate. However, if the voltage does saturate, the desired derivative term cannot be achieved. Therefore, the resultant current no longer tracks the MTPA curve, and then efficiency is not ideal.

To address this issue, an optimal torque rate limit is used to maximize bus voltage utilization. By discretizing Eqs. 15 and 16,

$$V_d[k] = R_s I_d[k] - \omega_e L_q I_q[k] + \frac{L_d}{T_s}(I_d[\mathrm{k}+1] - I_d[\mathrm{k}]) \qquad \text{Eq. 17}$$

$$V_q[k] = R_s I_q[k] + \omega_e L_d I_d[k] + \frac{L_q}{T_s}\left(I_q[\mathrm{k}+1] - I_q[\mathrm{k}]\right) \qquad \text{Eq. 18}$$

$$V_s[k] = \sqrt{V_d[k]^2 + V_q[k]^2} \qquad \text{Eq. 19}$$

The d-axis and q-axis current references are functions of torque, speed and bus voltage and can be obtained from control law equations or LUTs that satisfy these equations:

$$I_d[k] = f_d(\omega_m[k], V_{dc}[k],\ \tau[k]) \qquad \text{Eq. 20}$$

$$I_q[k] = f_q(\omega_m[k], V_{dc}[k],\ \tau[k]) \qquad \text{Eq. 21}$$

$$I_d[k+1] = f_d(\omega_m[k+1], V_{dc}[k+1],\ \tau[k+1]) \qquad \text{Eq. 22}$$

$$I_q[k+1] = f_q(\omega_m[k+1], V_{dc}[k+1],\ \tau[k+1]) \qquad \text{Eq. 23}$$

Since speed ω_m and bus voltage V_{dc} do not change significantly in one sampling period, $\tau[k+1]$ can be swept from minimum and maximum torque and $I_d[k]$, $I_q[k]$, $I_d[k+1]$, $I_q[k+1]$ can be used to derive $V_s[k]$. Values of $\tau[k+1]$ must be chosen for the controller which satisfies $V_s[k] = V_{dc}$. In this manner, V_s is maximized while

satisfying a control law using f_d and f_q functions. The term $\tau[k+1]$ can then be used to rate limit the torque command.

5.2 Deadbeat Controller

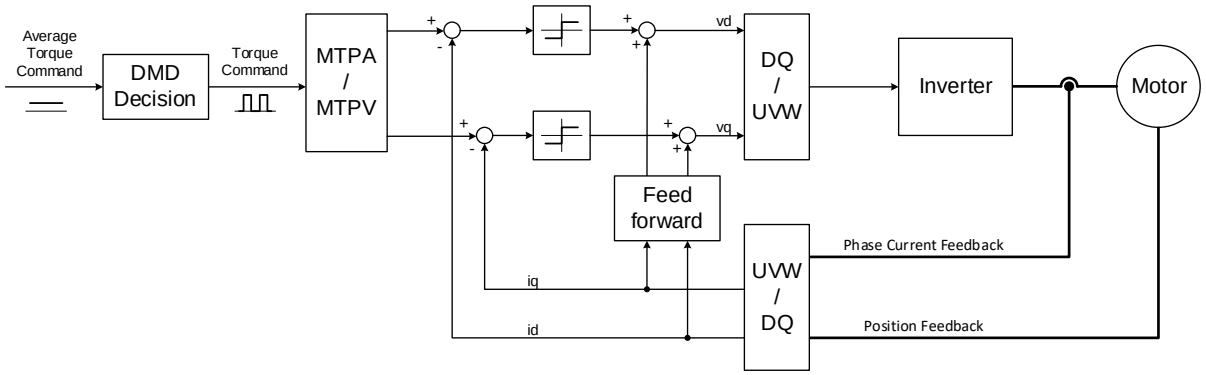

Fig. 13 Control system diagram.

Deadbeat control is used as the current controller. It has a very fast response speed, the bandwidth of which is limited only by the bus voltage or controller output limit. During saturation, the torque may transition to steady state command sub-optimally if ramp rates of the commands are not limited. Therefore, the optimal rate ramps are calculated for the commands that results in maximum bus voltage utilization, critically saturating deadbeat controller output during transients. This control structure ensures maximum voltage usage and that the state trajectory stays on MTPA, MTPL, or MTPF paths even for transients. This may not be possible with PI controllers as delays due to integrator can lead to underutilization of bus voltage. The proposed method is a feedforward and inverse model approach for tighter controller as shown in Fig. 13, thereby eliminating any integrators in the control loop.

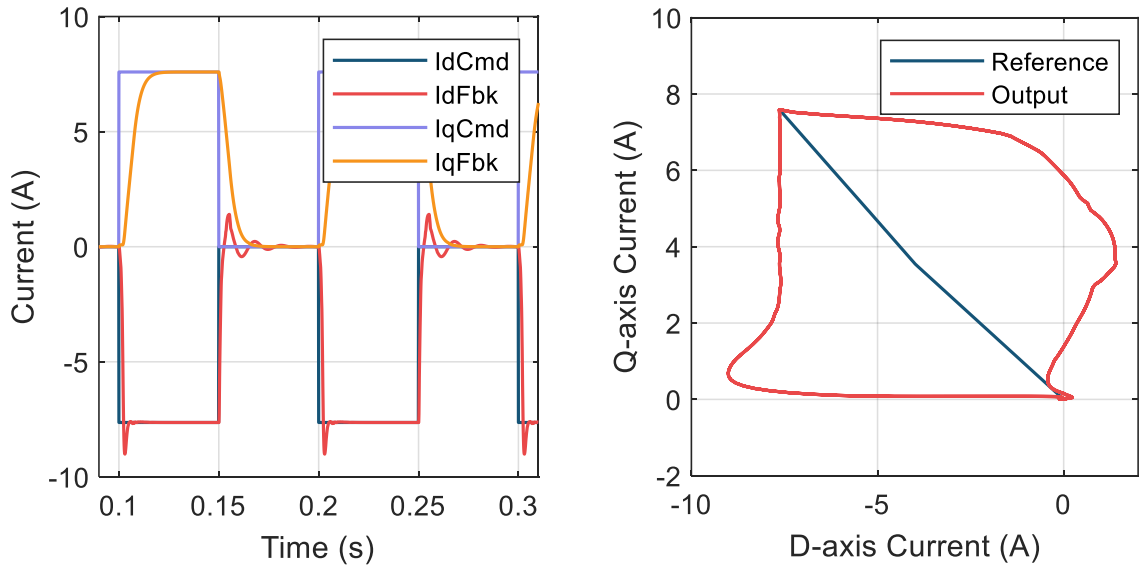

Fig. 14 Simulation results of conventional PI controller: (a) current waveform; (b) current trajectory.

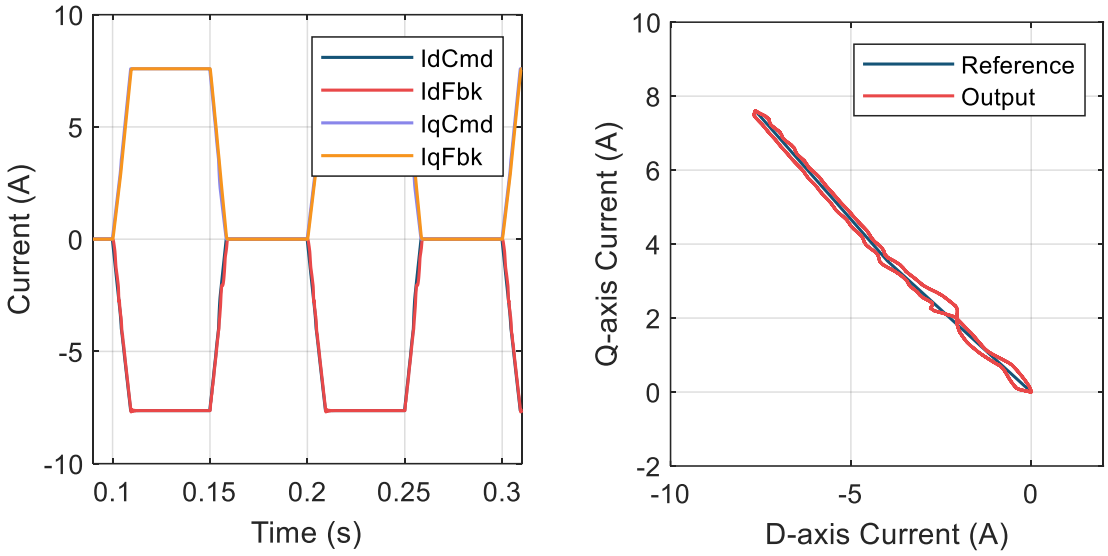

Fig. 15 Simulation results of proposed deadbeat controller: (a) current waveform; (b) current trajectory.

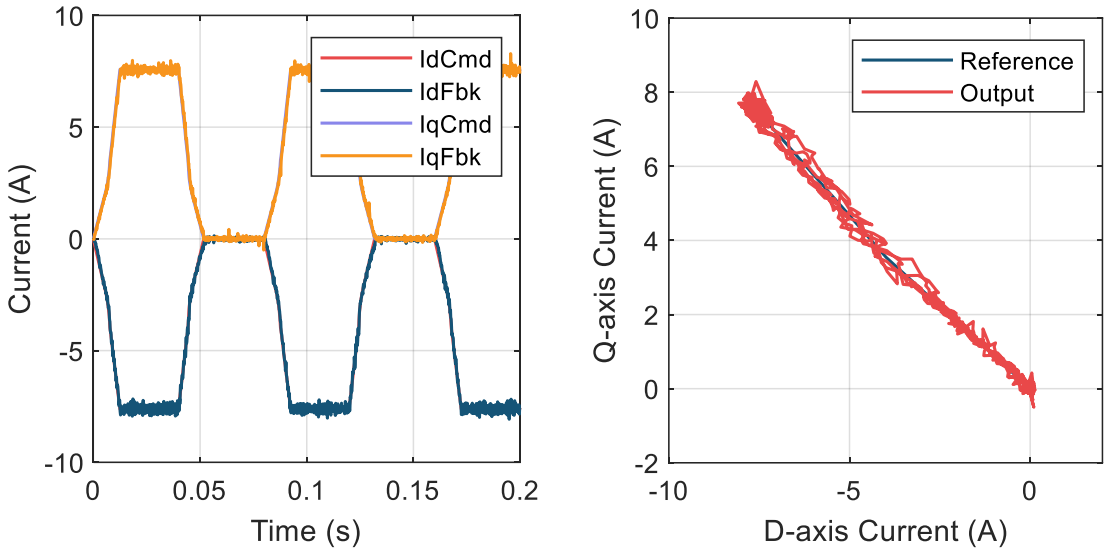

Fig. 16 Experimental results of proposed deadbeat controller: (a) current waveform; (b) current trajectory.

A comparison of current waveforms of different control strategies are shown in Fig. 14, Fig. 15, and Fig. 16. The simulated result of conventional PI controller shows latency, overshoot, and current that does not follow the MTPA trajectory. In contrast, the simulated and experimental results of the proposed deadbeat controller exhibit perfect tracking of the MTPA trajectory.

6 NVH Simulation

Of critical importance to DMD implementation is operating within limits of Noise, Vibration and Harshness (NVH). Modulating the torque on and off may cause vibration and/or acoustic noise. In order to ensure transparent operation for vehicle occupants, Tula is confirming DMD algorithms on a retrofitted Chevy Bolt. The original 150kW IPM motor is being replaced with a newly developed SynRM. In depth simulation of vibrations has been conducted to predict the torsional vibration and develop control techniques that will minimize vibration while maintaining maximum efficiency gains.

6.1 Drivetrain Sensitivity

Frequency spectrums of the torque input modulations with various duty cycle are shown in Fig. 17. Torque waveform has 200Nm peak value, and 40Hz periodic frequency. The ramp rate is set to the maximum value based on the inverter's capability to minimize electrical transient losses. The modulation period defines the waveform's periodic nature, and together with the duty cycle and torque amplitude, affects the vehicle's vibration response. With different duty ratios, the amplitudes of harmonics also vary.

A 1-D driveline model of an EV is used in simulation. It consists of rotational inertias, compliance, and damping that are either calculated from the component's geometry or derived experimentally. The model's input is a torque waveform, and its output is the torsional vibration at any rotational element.

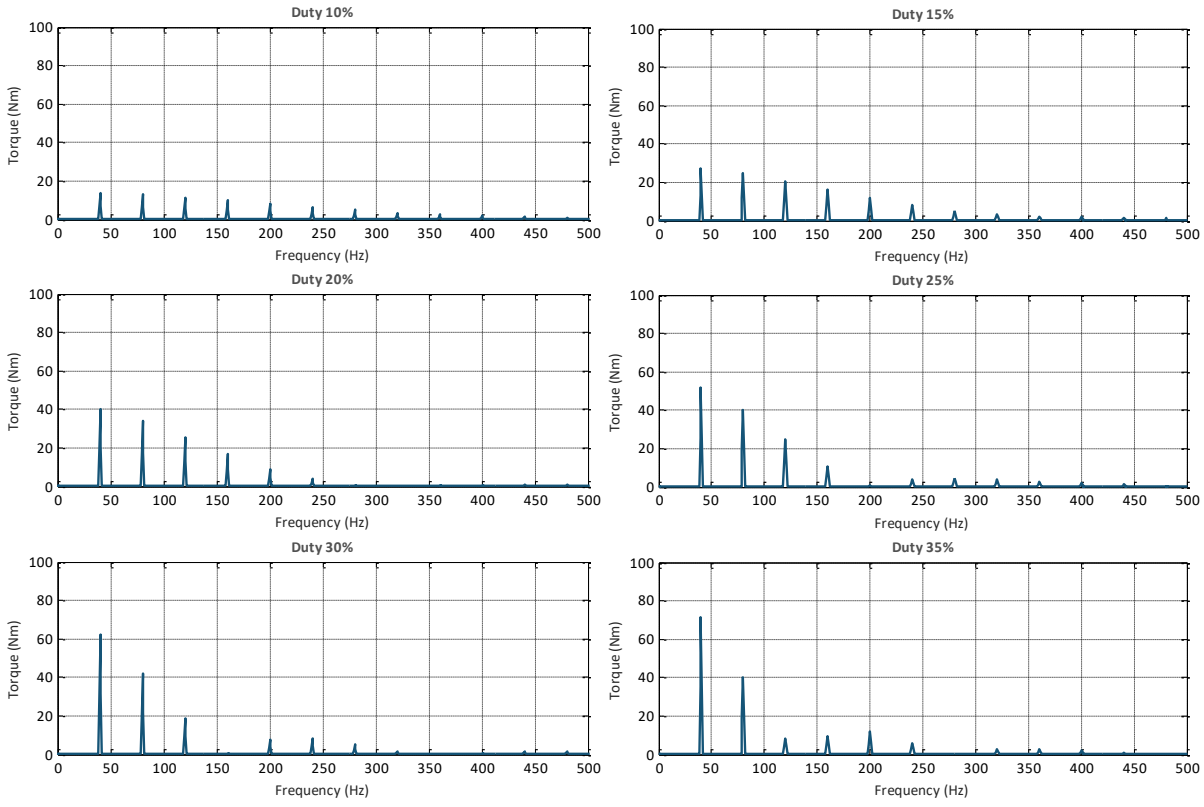

Fig. 17 Frequency spectrums of 200Nm DMD torque input with various duty cycles.

The modulating torque introduces periodic excitation. It propagates to the interior of the vehicle through the driveline system, causing torsional vibration. With no isolation device between the electric machine and the vehicle wheels to mitigate the periodic disturbances, torsional speed oscillations are expected to be observed.

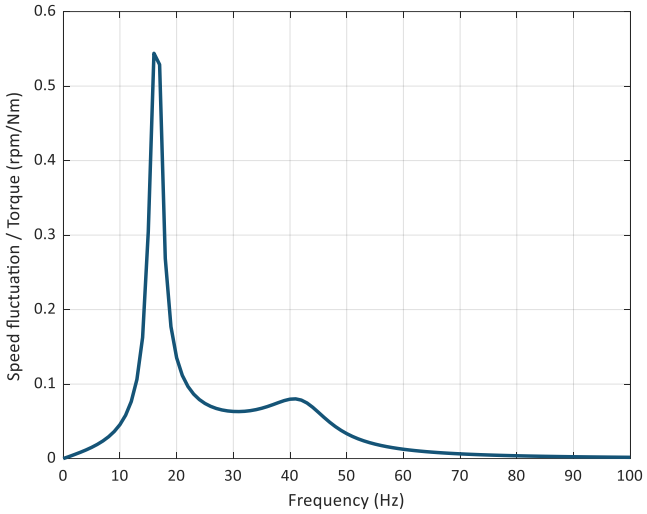

Fig. 18 Driveline Sensitivity.

The driveline sensitivity is depicted in Fig. 18. At approximately 16 Hz, the torsional response of the driveline is quite sensitive, so any modulating torque waveforms close to that frequency would result in objectionable vibration feel. Fortunately, the frequencies of modulation are able to be calibrated in DMD and these sensitive oscillation frequencies can be easily avoided.

6.2 DMD Torque Modulation Strategies

Two strategies are proposed to mitigate torsional vibration perception. The first is to intermittently apply a time delay to the torque modulation signal equal to half its period, in other words, switching the modulation waveform phase between 0 and 180 degrees. Fig. 19 shows an example of this phase shift strategy implementation where the torque pulse switches phase every 3 cycles.

The phase shift pulse has an intrinsic periodic nature with a specific frequency that interacts with the original pulse frequency, and thus adds frequency content that might be perceived as objectionable. The phase shift pulse frequency f_p depends on the original pulse frequency f_m, the number of cycles that the signal stays in or out of phase a, and the phase shift transition rate r.

$$f_p = \frac{1}{2a + \frac{1}{r}} \cdot f_m \qquad \text{Eq. 24}$$

Parameters are needed to be identified to minimize the resulting overall Root-Mean-Square (RMS) values of all frequencies of torsional vibration, so that it becomes lower than the corresponding results of the fixed frequency and fixed phase strategy. Fig. 20 compares a fixed frequency torque pulse at 40Hz with and without phase shift. From

the simulation, it is known the phase shift strategy reduces 35% of the axle torsional vibration.

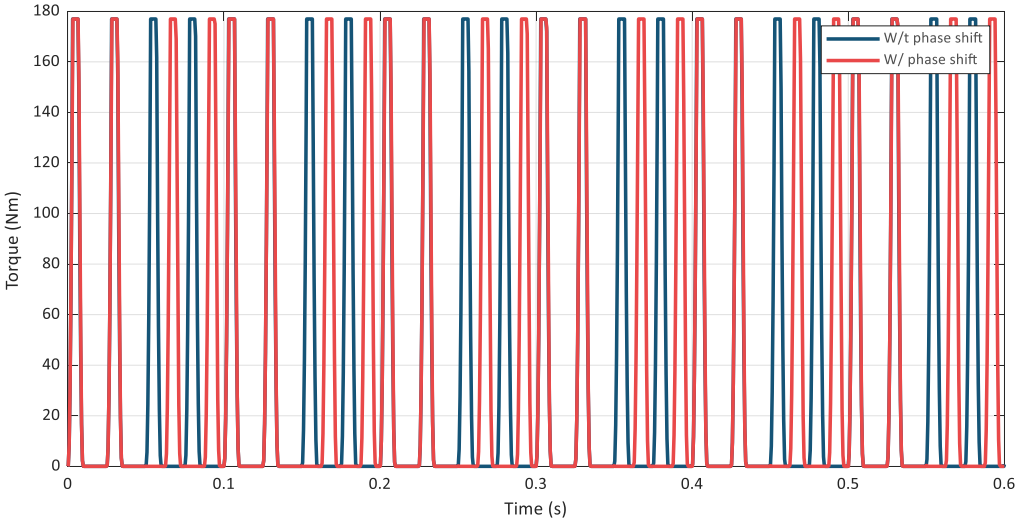

Fig. 19 An example of torque pulse phase shifting.

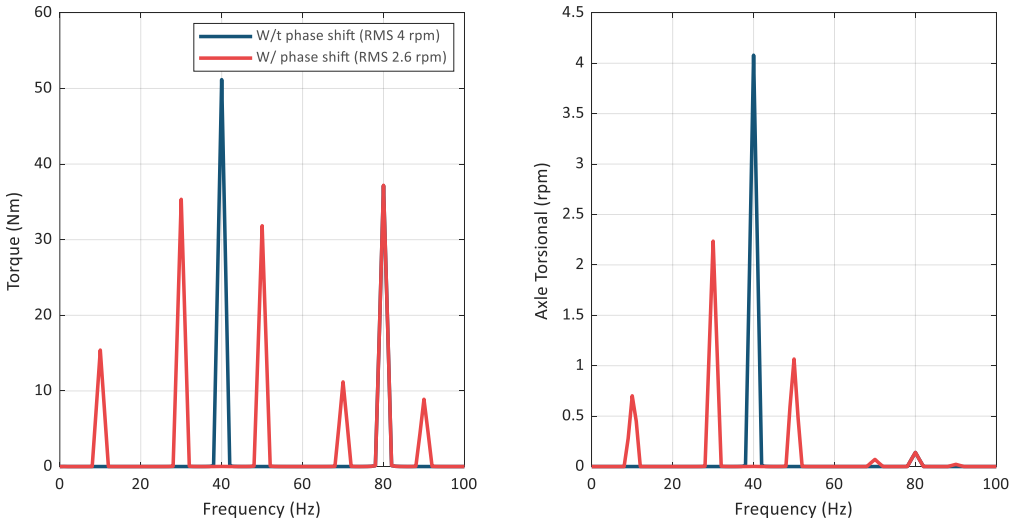

Fig. 20 Axle torsional vibration spectrum comparison with and without phase shift: (a) input torque spectrum; (b) axle torsional vibration spectrum.

Another strategy disrupting the fundamental pulse peak is to continuously vary the pulse frequency, while keeping the same duty ratio. Fig. 21 shows a comparison between fixed frequency of 32 Hz, and variable frequency between 4 Hz and 40 Hz. The resultant torsional vibration spectrum is shown in Fig. 22. From the figure, the proposed strategy reduces vibration by 22%.

Alternative strategies are being developed by Tula to maximize the impact of DMD, and all implementations of DMD will be accomplished in a manner in which NVH perception is comparable to baseline.

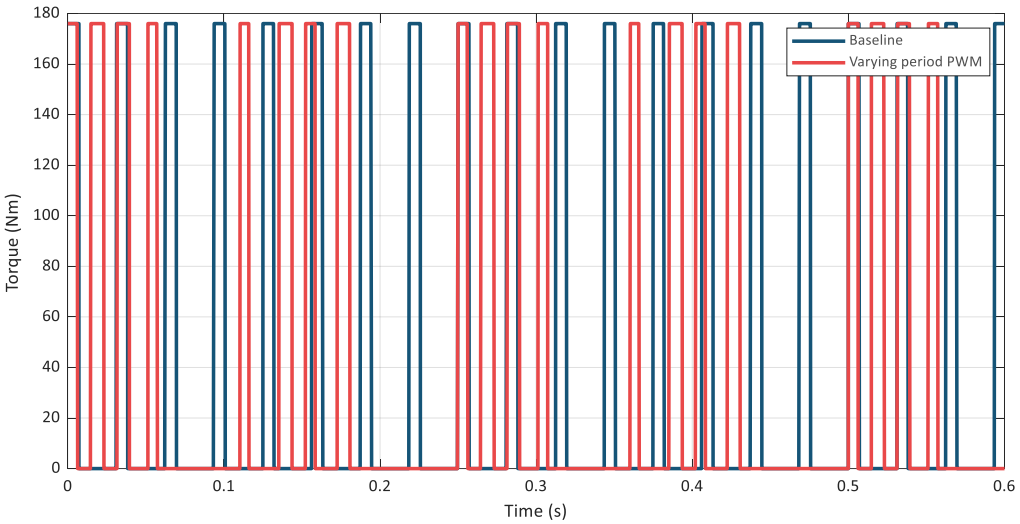

Fig. 21 An example of torque pulse frequency changing.

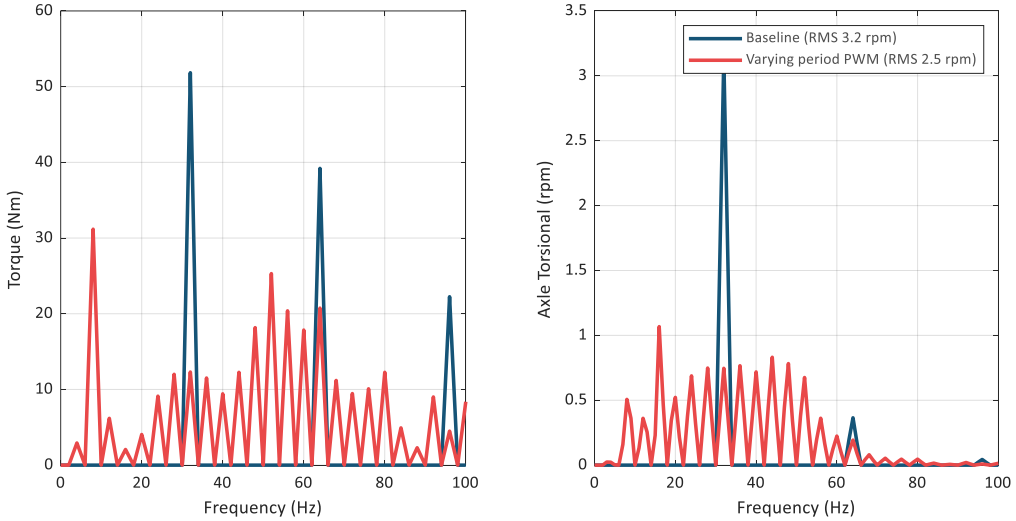

Fig. 22 Axle torsional vibration spectrum comparison with and without pulse frequency change: (a) input torque spectrum; (b) axle torsional vibration spectrum.

7 Drive Cycle Efficiency

To determine the effectiveness of efficiency improvement by DMD, drive cycle simulation has been done by using a 150kW SynRM's FEA data from JMAG-designer. The overall efficiency gain as a function of torque and speed is shown in Fig. 23. At torques of around 70Nm and below, a gain of at least 2% efficiency is seen. At the lowest torques, improvements exceeding 20% can be seen. These gains are substantial considering they are the result of an easily implementable software strategy.

These gains are translated into gains on the WLTP cycle in Fig. 24. The total energy usage is reduced by over 2% by implementing DMD electric motor control. This

improvement allows for longer ranges or smaller batteries that will have a substantial impact on electric vehicles.

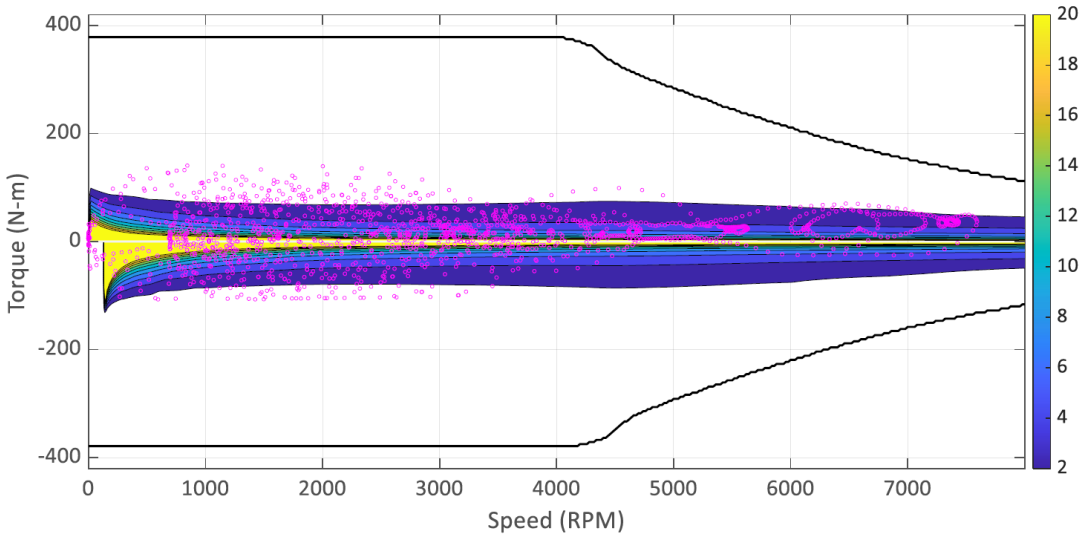

Fig. 23 System efficiency improvements for DMD, overlaid with WLTP operating points.

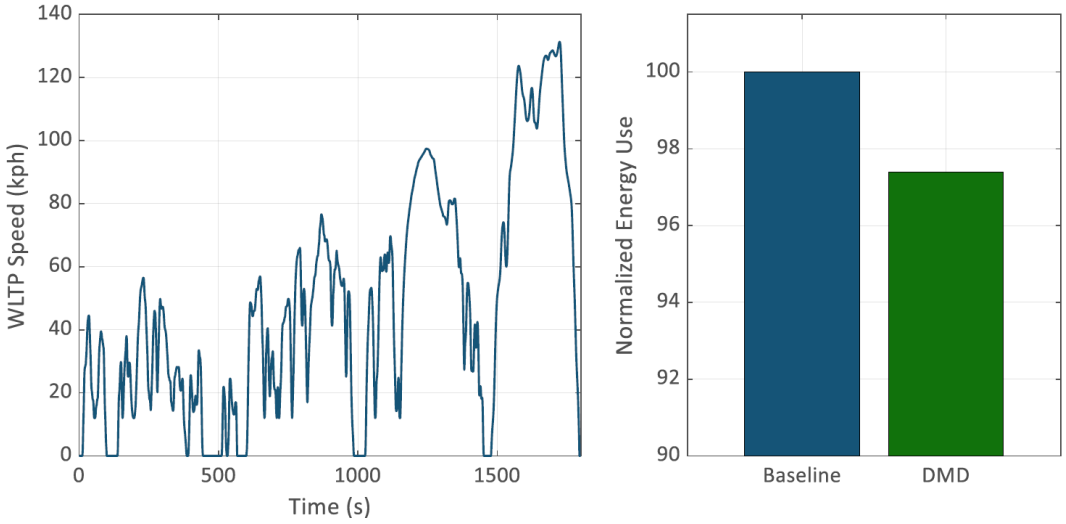

Fig. 24 Relative energy usage on WLTP cycle.

8 Impacts of Dynamic Motor Drive

Dynamic Motor Drive (DMD®) is a control strategy optimizing motor and inverter system efficiency. It requires no additional hardware and is easy to implement in software with IP licensed from Tula. Vibration issues can be solved by using industry-proven techniques developed with Tula's Dynamic Skip Fire (DSF®) technology. The strategy makes use of a very fast response speed of the proposed current controller to realize optimal efficiency at both steady and transient states. Significant efficiency improvements on relevant drive cycles are achieved, helping to reduce or eliminate rare earth material dependence and downsize the battery capacity required.

9 References

[1] Satterley, N., 2015.
Economic cost of the health impact of air pollution in Europe.
World Health Organization.
Retrieved from https://www.euro.who.int/en/media-centre/events/events/2015/04/ehp-mid-term-review/publications/economic-cost-of-the-health-impact-of-air-pollution-in-europe

[2] Fritschi, L., Brown, A., Kim, R., Schwela, D., and Kephalopoulos, S., 2011.
Burden of disease from environmental noise: Quantification of healthy life years lost in Europe.
World Health Organization.
Retrieved from https://www.euro.who.int/en/health-topics/noncommunicable-diseases/cardiovascular-diseases/publications/2011/burden-of-disease-from-environmental-noise.-quantification-of-healthy-life-years-lost-in-europe

[3] NASA.
Climate Change: How do we know?
Retrieved March 4, 2021, from https://climate.nasa.gov/evidence/

[4] IEA, 2020.
Coal-Fired Power.
Retrieved February 20, 2021, from https://www.iea.org/reports/coal-fired-power

[5] U.S. Department of Energy, 2011.
Critical Materials Strategy.
Retrieved March 6, 2021, from U.S. Department of Energy: https://www.energy.gov/sites/prod/files/2019/06/f63/DOE_CMS2011_FINAL_Full_1.pdf

[6] Adamas Intelligence, 2018.
Spotlight On Dysprosium.
Adamas Intelligence.
Retrieved from https://www.adamasintel.com/report/rare-earth-magnet-market-outlook-to-2030/

[7] Adamas Intelligence, 2019.
Rare Earth Elements: Small Market, Big Necessity.
Adamas Intelligence.

[8] Younkins, M., Carvell, P., and Fuerst, J., 2021.
Dynamic Motor Drive: Optimizing Electric Motor Controls to Improve Efficiency.
42nd International Vienna Motor Symposium.

[9] Mohr, M., and Fuchs, F.W., 2005.
Comparison of Three Phase Current Source Inverters and Voltage Source Inverters Linked with DC to DC Boost Converters for Fuel Cell Generation Systems.
European Conference on Power Electronics and Applications.

[10] Petrescu, L., Ionita, V., Cazacu, E., Petrescu, C., 2017.
Steinmetz' Parameters Fitting Procedure for the Power Losses Estimation in Soft Magnetic Materials.
International Conference on Optimization of Electrical and Electronic Equipment (OPTIM) & Intl Aegean Conference on Electrical Machines and Power Electronics (ACEMP).